Open access • Journal Article • DOI:10.1088/0960-1317/16/8/014

Design, kinematic modeling and performance testing of an electro-thermally driven microgripper for micromanipulation applications — Source link

Marco J F Zeman, Marco J F Zeman, Evgueni V. Bordatchev, Evgueni V. Bordatchev ...+1 more authors

Institutions: University of Western Ontario, National Research Council

Published on: 01 Aug 2006 - Journal of Micromechanics and Microengineering (IOP Publishing)

Topics: Microactuator

Design, kinematic modeling and performance testing of an electro-thermally driven microgripper for micromanipulation applications

Zeman, Marco J.F.; Bordatchev, Evgueni V.; Knopf, George

Publisher's version / Version de l'éditeur:
https://doi.org/10.1088/0960-1317/16/8/014
Journal of Micromechanics and Microengineering, 16, pp. 1540-1549, 2006

Design, Kinematic Modeling and Performance Testing of a Microgripper for Micromanipulation Applications

Marco J.F. Zeman[1,2], Evgueni V. Bordatchev[2,1], George K. Knopf[1]

[1] Department of Mechanical & Materials Engineering
The University of Western Ontario
London, Ontario, Canada N6A 5B9

[2] Integrated Manufacturing Technology Institute
National Research Council of Canada
800 Collip Circle, London Ontario, Canada, N6G 4X8

Submitted to: Journal of Micromechanics and Microengineering, Institute of Physics

Classification numbers: 07.10.Cm, 85.80.Fi. 85.85.+j

Abstract

Microgripping systems incorporate miniature end-effectors used to manipulate micro-sized objects such as tiny mechanical parts, electrical components, biological cells, and bacteria. This paper presents a thorough study of the design, kinematics, and static and dynamic performance, including electro-thermo performance characteristics, of the new microgripping system. The developed microgripper had a monolithic design which consisted of a combination of an in-plane electro-thermally driven microactuator and a compliant tweezing mechanism. The kinematics of the microgripper was studied as a kinematic transformation of input linear actuation motions into output tweezing displacements and compared with microgripper prototypes fabricated from 25 μm thick nickel foil by using laser micromachining technology. The static, dynamic, and electro-thermal characteristics of the system performance were analyzed with respect to actual actuation motions, tweezing displacements, voltage, power, electric resistance, and overall temperature under constant applied current within a range of {20, 40, ..., 160} mA. Maximum tweezing displacements of 47.461 μm (tweezing gap of 94.922 μm) were achieved under an applied current of 160 mA for a fabricated microgripper having an angle of the long rigid link to the horizontal α_0' = 60°, an angle of the short rigid link to the horizontal β_0' = 60°, and a transform coefficient K = 1.731. The repeatability and reliability of the fabricated microgripper were also tested along with capability to grip, hold and release a 110 μm diameter glass bead proving that this microgripper can be utilized as a grasping end-effector for micromanipulation, microrobotic and microassembly applications.

1. Introduction

Microgrippers and microtweezers have been used as miniature end-effectors in a variety of applications including mechanical micro-assembly, micro-robotics and biological cell manipulation. A diversity of microgripper designs is necessary to carefully grasp and handle these fragile micro-objects with geometric dimensions below one hundred micrometers. Consequently, the microgripper is a complex micro-electro-mechanical system, the performance of which depends upon the material properties, method of actuation, part geometry, and the kinematic behaviour of the design.

Gripper-type micro-electro-mechanical systems (MEMS) require a sophisticated method of actuation which is based on fundamental material properties in order to achieve a gripping motion. The most common microactuation methods are based on electrostatic, piezoelectric, electro-thermal, and shape memory alloy (SMA) effects. Typical electrostatic actuators require very high voltages, as demonstrated by the electrostatic gripper created by Lee *et al.* [1] requiring 250 V to create an electric field across two electrostatic electrodes to grab a glass bead with a diameter of 170 μm, where a third electrode was actuated electro-thermally using 100 mA to push and release the glass bead. Even finger-like comb drive microactuators require higher voltages in the range of 80V, where only relatively small displacements of up to 20 μm were observed [2]. Similarly, piezoelectric actuators also require high voltages. The microgrippers made of superelastic alloy created by Menciassi *et al.* [3] required 150V to achieve a tip displacement of 395 μm. Kohl *et al.* [4-5] created an SMA microgripping system which relied on one-way shape memory and therefore required two separate mechanisms of actuation for closing and opening of the gripping jaws. The device achieved a maximum stroke of 300 μm with applied power of 80 mW. The actuation components in this design reach a maximum temperature of 59 °C. A larger 1.7 cm long SMA microgripper introduced by Roch *et al.* [6] could achieve a tip displacement of 250 μm with a 1 V and 0.9 A source.

This paper presents a new microgripper design, its kinematics, and also the experimental performance on several fabricated microgrippers. Two methods of testing are explored - constant voltage and constant current controls. By better understanding the effects of the testing methods on the microgripper, proper control and predictable results are achieved. Several electro-thermo-dynamic characteristics including applied current/power, averaged temperature, actual resistance, and gripping gap, are studied. In addition, the dynamics of the proposed microgripper is studied using a step response function and then was compared with the simulation results obtained from the kinematic model.

2. Microgripper Design

In this paper, a design concept for the microgripper is considered in order to create a functional microgripper capable of manipulating tiny (<150 μm) objects such as glass beads, hair fibers, micro objects and more. The concept of the functional microgripper design consists of compliant gripping mechanism coupled with an in-plane microactuator as seen in Figure 1.

The microgripper is a monolithic 2-D structure where the microactuator and the compliant gripping mechanism are linked using compliant flexural hinges. The microactuator is based on a multi-cascaded approach [7, 8, 9] and has seven actuation units. The design consists of a pair of identical cascaded actuation structures. Each actuation structure has seven actuation units connected serially which increases the vertical output displacement. The actuation unit is composed of two V-shaped (chevron type) actuation beams and one constraining beam. A pair of vertically parallel actuation structures is linked together by a horizontal motion platform. At the bottom of the microactuator, two fixed electrical pads are located to apply power across the microactuator.

Before fabricating and testing the functional microgripper which is used for practical micromanipulation, a simplified microgripper design (see Figure 1a) is developed to validate the design concept of the microgripping system. Several simplified microgrippers with design parameters are designed, fabricated, and tested in order to compare to the results obtained in the kinematic simulation. In contrast to the functional microgripper (see Figure 2a), the simplified microgripper design contains straight long rigid links as opposed to curved long rigid links in the gripping mechanism. The straight long beams in the simplified design in this comparative study are not practical for fabrication and for micromanipulation applications because the overall height of the gripping mechanism becomes too long.

The design concept of the compliant gripping mechanism is identical for both the functional and simplified microgripper. The compliant gripping mechanism consists of a pair of gripping arms which represent a mirror image of each other and are reflected about the vertical center of the microgripper. Each gripping arm has short and long rigid links, three compliant flexural hinges, and a gripping jaw. Each gripping jaw has a concave shape creating internal circular cavity with a diameter of 100 μm for holding rounded micro objects. The long rigid link ends with a gripping jaw and is linked to a fixed physical anchor. One end of the short rigid link is joined to the motion platform of the microactuator and the other is joined to the long rigid link. All joints between the links and microactuator are connected by compliant flexural hinges.

The design of the microgripping mechanism requires that all joints mimic a rotational joint by using compliant flexural hinges. These flexural hinges are 10 μm wide at their most narrow point (see Figure 1b). In monolithic devices, flexural hinges are compact, easy to fabricate using laser micromachining, do not require lubrication, and have no frictional losses. Although, flexural hinges do not provide pure rotation due to the complex deformation of the flexure, and the rotational center of the hinge is not fixed during rotation, they are only ideal for structures that require small rotational displacements [10] such as proposed microgripper. The joint between the microactuator and the compliant mechanism is composed of two flexural hinges, one for each arm of the microgripper, and is affected by heat conduction from the adjoining microactuator, creating other complexity to this particular flexural hinge.

Upon applying a voltage across the fixed electrical anchors of the microactuator to form an electrically closed loop, an output displacement is generated for the motion platform as a summation of all seven actuation units in one cascaded structure. Figure 2a shows generalized kinematics of the actuation unit where the direction of motion of the actuation beams can be outward (stretching mode) or inward

(shrinking mode), depending on whether the actuation beams are thermally expanding or contracting, respectively. A perfectly symmetric monolithic structure will ensure a symmetrical distribution of voltage, temperature, and displacement along the vertical center of the microgripper.

Each actuation unit of the microactuator is designed to be symmetrical about the vertical and horizontal axes. As it shown on Figure 2b, the symmetrical design provides identical actuation beam resistances for R_1 to R_4 which allows the input current to flow uniformly through the actuation beams, causing voltages V_1 and V_2 to be equal. The schematic of a single actuation unit is synonymous with that of a balanced Wheatstone bridge. Since the actuation beams are the thinnest features of the design with a cross-section of 10 x 25 μm (width to thickness), then they have a high electrical resistance which increases the Joule heating and physical expansion. The constrainer beam accounts for the resistance R_5 which has no voltage or current across it because the voltages at nodes 1 and 2 are identical. As a result, the constrainer's function is purely mechanical, to be strong enough to restrain the direction of motion in the desired vertical direction and to mechanically strengthen each actuation unit.

When current flows through the microactuator, thermal expansion causes an in-plane displacement pushing the motion platform upward and consequently pushing the long rigid links outward, opening the gripping jaws. Once the electrical current is removed, the microactuator cools and shrinks, returning the gripping jaws to their originally closed position. Due to the design and voltage/current distribution symmetry, the gripping mechanism does not provide a closed electrical path, no current flow through the gripping mechanism, and the entire compliant gripping mechanism has a uniform voltage which is the same as the voltage of the motion platform. Thermal isolation at the gripping jaws is achieved by preventing thermal heating due to current flow in the compliant gripping mechanism, not affecting temperature sensitive objects which are being manipulated.

The microgrippers studied in this paper were fabricated from a 25 μm thick pure nickel foil using laser microfabrication technology [7, 9, 11]. The parameters of the laser-material removal process, such as laser power, pulse repetition rate, working distance, and feed rate, were optimized in order to obtain a 10 μm cut width and to achieve accuracy and precision of the fabricated prototype within +/– 1 μm.

3. Kinematic Modeling

Figure 3 shows a generalized kinematics of the microgripping system as a functional relationship, represented by the transform coefficient, K, between the in-plane linear actuation motions of the microactuator's platform upon actuation (input), $h(t)$, and tweezing displacements of one gripping jaw (output), $x(t)$, as it shown in Figure 3. The vertical motion, $y(t)$, of the gripping jaw is not considered in this paper since it is compensated by the y-motion of the entire microgripper in practical applications. The compliant microgripping mechanism has two functions: it geometrically transforms vertical input actuation motions into output horizontal tweezing displacements and it amplifies the tweezing displacements. By

providing a kinematic model of the microgripping system, the distance between gripper jaws can be predicted with respect to a given displacement achieved by the linear microactuator.

The transform coefficient is defined by several geometric design parameters of the microgripper's kinematic structure shown in Figure 4 and consisted of a complex combination long and short rigid links, two rotary joints and slider. The geometric design parameters include the initial vertical offset, h_0, the angle of the long rigid link to the horizontal, α_0', the angle of the short rigid link to the horizontal, β_0', and the horizontal distance between the one end of the long rigid link and the end of the short rigid link attached to the moving platform of the microactuator, ℓ_0. In general, the tweezing displacements, $x(t)$, can be expressed as

$$x(t) = K \cdot h(t), \text{ where } K = K(h_0, \alpha_0', \beta_0', \ell_0). \quad (1)$$

In general, the kinematic model of the microgripping mechanism has the three different case scenarios considered for the initial vertical offset distance of the linear microactuator, which are $h_0 = 0$, $h_0 < 0$, and $h_0 > 0$. A detailed kinematics of a microgripping mechanism is given in Figure 5 for the case where $h_0 > 0$ at $t = 0$, and after actuation at any time t. For all three case scenarios for h_0, a generic model is created in order to locate the motion of the gripping jaw. Using any values for the design parameters h_0, α_0', β_0', and ℓ_0, which are specified by the designer, equation (2) is used to calculate the tweezing displacements of one gripping jaw, $x(t)$, with respect to the input actuation motion, $h(t)$ as

$$x(t) = l_0 - \frac{\ell_0}{\cos\alpha_0'} \cos\left[\tan^{-1}\left(\frac{h(t)+h_0}{\ell_0}\right) + \cos^{-1}\left(\frac{b^2 + c_1^2 - a^2}{2bc_1}\right)\right] \quad (2)$$

where:

$$\alpha_0'' = \beta_0'' = \tan^{-1}\left(\frac{h_0}{\ell_0}\right);\ \alpha_0 = \alpha_0' - \alpha_0'';\ \beta_0 = \beta_0' + \beta_0'';$$

$$\gamma_0 = 180 - \alpha_0 - \beta_0;\ c_1 = \sqrt{(h(t)+h_0)^2 + \ell_0^{\,2}};$$

$$a = \frac{c_0 \sin\alpha_0}{\sin\gamma_0};\ b = \frac{c_0 \sin\beta_0}{\sin\gamma_0};\ c_0 = \left|\frac{h_0}{\sin\alpha_0''}\right|.$$

The microgripper's kinematic performance was simulated for design parameters h_0 = 0 μm, α_0' = {10°, 20° ... 80°}, β_0' = {10°, 20° ... 80°}, and ℓ_0 = 1200 μm and some simulation results shown in Figure 6. Analysis shows that α_0' has the largest impact on magnification of the tweezing displacements whereas β_0' has little effect, for example, for input displacement h = 20 μm and α_0' = 40°, changing β_0' from 10° to 80° produces increase of the tweezing displacements from 16.9 μm to 19.0 μm for a total of

2.1 μm, which is 12.4% magnification (see Figure 6a). Contrary, for β_0' = 40°, changing α_0' from 10° to 80 ° generates a magnification of 21 times increasing tweezing displacements from 5.1 μm to 112.3 μm for a total of 107.2 μm (see Figure 6b). The simulation results are used in Section 5 for comparative study with experimentally obtained results from performance testing.

4. Experimental Setup and Procedures

The experimental setup for evaluating the performance characteristics of the fabricated microgripper is shown in Figure 7. The setup consisted of a power supply (Agilent A3631A), 1 Ω power resistor, digital oscilloscope (LeCroy WaveRunner, LT354), optical microscope (Olympus, SZX12) with a CCD camera under Vision Gauge™ software control, in-house software control with NI Vision Builder™ vision analysis, and a desktop computer. Three parameters of microgripper's performance were measured simultaneously in time and space domain – actual voltage across the entire electric circuit including microactuator and power resistor through the channel 1 (CH1) of the oscilloscope, applied current calculated through the measured voltage across the constant power resistor and channel 2 (CH2) of the oscilloscope, and actuation motions, $h(t)$, and tweezing displacements, $x(t)$, through the optical microscope.

The microgripper was mounted on a small glass plate glued to a plastic container, and it was wired to a standard socket for electrical connections as shown in Figure 8. A standard multimeter was used to measure the electrical resistance and was found to be 2.7 Ω for the seven actuation unit microgripper. The total resistance of all connecting wires was 0.4 Ω.

Nine simplified microgripper prototypes were designed and fabricated with all possible combinations between α_0' = {30°, 40°, 60°} and β_0' = {30°, 40°, 60°} while keeping the design parameters h_0 = 0 μm and ℓ_0 = 1200 μm fixed. All microgrippers had identical microactuators with seven actuation units. The performance evaluation of the microgrippers involved the following two testing methods used during experimentation.

The procedure for the performance testing experiments involved the following steps. When prompted to start, the in-house developed software on the PC sent a signal to the power supply to output a driving step input current to the microgripper. Simultaneously, the voltage and current were recorded by the digital oscilloscope, and the images of the motion platform of the microactuator and the gripping jaws were captured by a CCD camera through the optical microscope and by the in-house developed software. Afterwards, actuation motions, $h(t)$, and tweezing displacements, $x(t)$, were extracted from the captured images using NI Vision Builder™ software.

As a result, performance characteristics of the fabricated microgrippers were obtained as step responses of the produced voltage, actuation motions, and tweezing displacements on applied constant current. Having step response functions allowed obtaining the following microgripper's electro-thermo-

dynamic, as a transient response, and static, as a steady state, performance characteristics:

- the step response functions under applied constant current,
- the actuation motions / tweezing displacements vs. applied current and power, and
- the calculated overall temperature and resistance vs. applied current.

To achieve smooth tweezing displacements for the microgripper, all testing experiments were performed under constant current control (CCC) scheme provided by the power supply where the desired current was set firm and the voltage across microactuator was generated in accordance to the actual resistance of the microactuator. CCC scheme prevents current spikes, burning of the microactuator, and displacement overshoot [12]. Figure 9 shows the typical electrical step response characteristics, such as, applied current, $I(t)$, and produced voltage, $V(t)$, and mechanical step response characteristics, e.g., actuation motion, $h(t)$, and tweezing displacement, $x(t)$, obtained under a CCC scheme. As it shown in Figure 9a, the applied current of 160 mA reaches its steady state (SS), I_{SS}, almost instantly with a transient response time, t_{TR}^{I}, of 40 ms. The voltage rises to a steady state, V_{SS}, of 1.6 V across the microgripper during 32.5 times longer response time, t_{TR}^{V}, of 1.3 s. Mechanical responses, $h(t)$ and $x(t)$, follow the dynamic behaviour of $V(t)$ having a transient response time of 2.4 s (see Figure 9b).

Note that during experiments all applied currents were kept below 160 mA, which is a functional limit for a microactuator with seven actuation units before buckling and overheating effects occur [12].

5. Experimental Results and Analysis

5.1 Static Performance

Figure 10 shows the actual measured static (steady state) performance of a simplified microgripper with design parameters of α_0' = 40° and β_0' = 40° under an applied current of 160 mA. The total gap between the gripping jaws is double the tweezing displacement, x_{SS}, since the tweezing displacements are always measured for a single gripper jaw. With an applied current of 160 mA and steady state voltage of 1.6 V, the total gap displacement is 32.4 μm.

During the experiments with the microgripper with the same design parameters above, the applied current from the power supply was increased within a range of {20, 40, …, 160} mA. For these currents, the power was calculated and the overall steady state (SS) performance of the microactuator and microgripper was measured in terms of actuation, h_{SS}, and tweezing displacements, x_{SS}, respectively. Figure 11 shows obtained static performance characteristics as actuation motions vs. applied power and current. The tweezing displacements exponentially increase, along with a linear increase in the applied current where a maximum x_{SS} of 16.2 μm was recorded for an applied current of 160 mA. These static performance characteristics of the microgripping system allow the user to choose optimal control

parameters to obtain and sustain desired tweezing displacements and forces in practical applications.

The microgripper has a monolithic structure fabricated from pure nickel foil and therefore it exhibits a change in resistance when undergoing a change in temperature causing change of the physical-mechanical properties and the thermal-expansion coefficient of the nickel [14, 15]. Since the cross-sectional area of the actuation beams in the microactuator is only 250 μm^2, a large increase in temperature and resistance is expected. A more detailed description of how the resistance and the overall temperature of the microgripper were calculated can be found in [12]. Figure 12 shows that both the calculated resistance and overall temperature increase exponentially with a linear increase in electric current. At 160 mA, a maximum resistance and temperature of 9.25 Ω and 369.03 °C were calculated, respectively.

The static performance of all fabricated microgrippers with different design parameters of α_0' = {30, 40, 60}° and β_0' = {30, 40, 60}° was tested in terms of h_{SS} and x_{SS}, and results were compared with simulated performance, $\hat{x}_{SS}$, for given (experimentally obtained) h_{SS} through static error estimation calculated as

$$\Delta x = \left| x_{SS} - \hat{x}_{SS} \right|, \tag{3}$$

$$\hat{x}_{SS} = K \cdot h_{SS}, \tag{4}$$

where K is the static transform coefficient obtained from the simulation results (see Figure 6).

Table 1 summarizes the results of kinematic simulation, e.g., $\hat{x}_{SS}$ and K, actual performance, e.g., h_{SS}, x_{SS}, and K_{SS}, comparative analysis in terms of difference between simulated and experimental results, e.g. Δx and ΔK. These results show good correlation between simulated and experimental data having a maximum error in prediction of a tweezing displacement of 0.6 μm with relative accuracy of 1.63% and a maximum deviation in prediction of a transform coefficient of 0.029 with relative accuracy of 1.69%. Therefore, the developed kinematic model (2) adequately describes static performance of micrograpping mechanism. Also, it is important to note that designed and fabricated flexural hinges do not introduce significant mechanical stiffness and resistance to tweezing displacements and sufficiently represent rotary joints in the developed kinematic model (see Figure 4).

5.2 Dynamic Performance

The dynamic performance of the fabricated microgrippers was studied based on the analysis of the transient response of the step response function with respect to actuation motions (input) and tweezing displacements (output). As an example, Figure 13 shows the dynamic step response under CCC testing with an applied current of 160 mA across the microgripper. During these tests, the actual actuation motions, $h(t)$, and tweezing displacements, $x(t)$, were measured, and the expected tweezing displacement, $\hat{x}(t)$, were calculated using Equation 2. The dynamic error, $\Delta x(t)$, was calculated as

$$\Delta x(t) = |x(t) - \hat{x}(t)|, \tag{5}$$

where

$$\hat{x}(t) = K \cdot h(t). \tag{6}$$

Note that since the geometry of the tweezing mechanism does not change during actuation, the transform coefficient is constant for particular design parameters, $K = K(t, h_0, \alpha_0', \beta_0', \ell_0) = const$.

The analysis of the electrical response of the microgripper (see Figure 9a) shows that the applied current rises instantly and produces voltage having an electrical transient response time of 1.3 s whereas the mechanical transient response time has 2.4 s duration (see Figure 9b). The difference in the response times is a result of the different electric and thermo-mechanical behaviours and characteristics where an additional delay of 1.1 s caused by the heating time and the thermal response of the microactuator.

During the transient state (see Figure 9b), the actual tweezing displacements, $x(t)$, are lesser than the simulated/expected tweezing displacements, $\hat{x}(t)$, causing the dynamic error, $\Delta x(t)$, with a maximum value of 2.5 μm due to the delay between the thermo-dynamic expansion of the microactuator and mechanical response of the gripping mechanism. The actuation beams expand due to the heating effect of the current flow and consequently causing softening of the material. This softening reduces the stiffness of the entire microactuator reducing the force that pushes the compliant mechanism upward. Eventually, the force pushing downward, due to the stiffness of the compliant gripping mechanism, matches the upward force of the thermally expanded microgripper during steady state (static performance). After all, microgripper reaches steady state when the natural convection of the heat from the actuation beams becomes constant, as shown when the dynamic error approaches zero at steady state.

Also, as it can be seen from Figure 9b, after 2.4 s, $h(t)$ and $x(t)$ come to a steady state since these displacements continue to increase slightly during the steady state as the current continues to heat the microactuator via electro-thermal heating. Eventually, if the higher current is left on for too long, the microactuator overheats and buckles. Therefore, leaving the power supply on for 5 s allows to achieve a steady state reaching a reasonable balance between large enough tweezing displacements and workable damage to the microgripper due to overheating.

5.3 Repeatability/Reliability Performance

To determine the endurance of the microgripper performance, a repeatability/reliability test was performed on a microgripper with design parameters of α_0' = 40° and β_0' = 40°. The microgripper was tested under two applied currents of 120 mA and 160 mA for a duration of 10 s of each testing period (0.1 Hz) with a duty cycle of 50% (applied current is ON and OFF for 5 s). A total of 250 testing periods were

performed for each applied current. During the test, tweezing displacements and actuation motions were recorded simultaneously for further analysis. The results of the repeatability/reliability testing shown in Figure 13. Under an applied current of 160 mA, which is a workable maximum, the microgripper's repeatability was constantly declining reaching a total decrease of tweezing displacements of 2.25 μm (14.7%). The source of this decrease is thermo-dynamic performance of a microactuator, which has poor repeatability/reliability under critical working conditions, e.g., total decrease of actuation motions of 2.3 μm (12.1%). Nonetheless, the microgripper was still able to maintain its shape with just a little discoloration occurring in the microactuator due to overheating. Decreasing an applied current improved microgripper's repeatability/reliability, e.g., under an applied current of 120 mA, the microgripper was performing tweezing displacements within a range of 0.4 μm due to variations within actuation motions of 0.5 μm.

5.4 Gripping-Holding-Realising Testing of the Functional Microgripper

In order to test microgripper's functional performance for gripping-holding-realising operations with a micro object, a functional microgripper with seven actuation units and specific design parameters, α_0' = 80° and β_0' = 40°, was fabricated. The functional microgripper had some minor design modifications in order to decrease the overall length of the microgripper, e.g., a long rigid link was bent for 5° at the hinge where the short rigid link meets the long rigid link. Decreasing length of the long link strengthens the microgripper's capability to manipulate an object since the gripper jaws locate closer to the flexural hinge (see Figure 1b) and therefore they have larger stiffness.

Figure 14 illustrates the steps of functional testing – gripping, holding and releasing of a glass bead with a diameter of 110 μm. Initially, the microgripper was actuated with a current of 160 mA to open tweezing jaws and internal cavity up to 135.2 μm with an actuation motions of 19.4 μm (see Figure 14a). After that, the glass bead was manually delivered towards the opened jaws by using a 3 degree-of-freedom stage and a micro-brush with a single natural fibre (see Figure 14b). When the glass bead was located between tweezing jaws, applied current was disconnected to close jaws, and the fibre was removed. The glass bead was hold between jaws by a tweezing force generated by a displacement and stiffness of the returning into initial position microactuator. On the last step – releasing, the microgripper was actuated with the identical parameters to release the glass bead. Upon release, gravity force exceeded the static friction between the glass bead and the thin gripping jaws, and the glass bead fell down due to the gravity force.

6. Summary and Conclusions

This paper presents a systematic study of the kinematics, static behaviour, as well as the electro-thermo-dynamic behaviour of a proposed microgripping system using its electrical and mechanical step responses on applied current. Microgripper's design consisted of a 2D monolithic structure with rigid links

that joined a microactuator shell and a compliant tweezing mechanism using compliant flexible hinges. Kinematic model of the tweezing mechanism was developed and analysed with respect to two major design parameters – the angle of the long rigid link to the horizontal, α_0', the angle of the short rigid link to the horizontal, β_0', within a range of α_0' = {10°, 20° ... 80°}, β_0' = {10°, 20° ... 80°}. Two types of microgripper, simplified – for comparison with kinematic simulation and functional – for gripping-holding-realising application testing, were fabricated from a 25 μm thick pure nickel foil using laser microfabrication technology. Nine simplified microgripper prototypes were designed and fabricated with all possible combinations between α_0' = {30°, 40°, 60°} and β_0' = {30°, 40°, 60°} while keeping the other design parameters unchanged. The static (steady state) displacements and electro-thermal characteristics of these microgrippers were studied under constant applied current within a range of {20, 40, ..., 160} mA and with respect to actual actuation/tweezing displacements, produced voltage/power, resistance and overall average temperature. For a microgripper prototype with design parameters of α_0' = 40° and β_0' = 40°, tweezing displacement of 16.3 μm (tweezing gap of 32.554 μm) were obtained under an applied current of 160 mA. This result agrees well with the predicted motion of 16.1 μm derived from the kinematic simulation. The repeatability and reliability of the fabricated microgripper was also tested along with it's capability to grip, hold and release a micro object.

The following conclusion can be drawn from these studies:

1. The microgripper being a complex actuation system, is both reliable and repeatable, and also capable of generating accurate tweezing displacements, e.g., with variations within 0.4 μm under an applied current of 120 mA.
2. The kinematic model can reliably predict the dynamic performance of the proposed microgripper and shows that the angle of the long rigid link to the horizontal is the most influential design parameter in order to increase tweezing displacements.
3. The microgripper delivers smooth tweezing displacements under the constant current control operation without an overshoot or destructive current/voltage spikes.
4. The fabricated microgripping system exhibits complex nonlinear electro-thermal characteristics. The microgripper significantly changed its resistance from 2.7 Ω at room temperature to a maximum resistance and temperature of 9.25 Ω and 369.03 °C, respectively.
5. Maximum tweezing displacements of 47.461 μm (tweezing gap of 94.922 μm) were achieved for design parameters α_0' = 60° and β_0' = 60°, and a transform coefficient K = 1.731.
6. The microgripper can be used for handling and manipulation of miniature components and objects, e.g., fabricated functional microgripper was able to grip, hold and release a 110 μm diameter glass bead.

Acknowledgements

This paper is the result of the collaboration between NRC-IMTI and The University of Western Ontario, London, Ontario, Canada. The authors thank Mahmud-Ul Islam, Director, Production Technology Research, NRC-IMTI, and Suwas Nikumb, Group Leader, Precision Fabrication Processes, NRC-IMTI, for their continued support in this work. The authors also appreciate the assistance of Hugo Reshef for his help in performing the laser fabrication. This study was partially supported by NSERC Discovery Grant R3440A01.

References

[1] S. E. Lee, K. C. Lee, and S. S. Lee, "Fabrication of an Electrothermally Actuated Electrostatic Microgripper," *International Journal of Nonlinear Sciences and Numerical Simulation*, Vol. 3, No. 4, 2002, pp. 789-793.

[2] B. E Volland., H. Heerlein, and I. W. Rangelow, "Electrostatically driven microgripper," *Microelectronic Engineering*, Vol. 61-62, 2002, pp. 1015-1023.

[3] A. Menciassi, A. Eisinberg, M. Mazzoni, and P. Dario, "A Sensorized μElectro Discharge Machined Superelastic Alloy Microgripper for Micromanipulation: simulation and characterization," *Proceedings of the 2002 IEEE/RSJ Intl. Conference of Intelligent Robots and Systems*, October 2002, Lausanne, Switzerland, pp. 1591-1595.

[4] M. Kohl, B. Krevet, and E. Just, "SMA Microgripper System," *Sensors and Actuators: A,* Vol. 97-98, 2002, pp. 646-652.

[5] M. Kohl, E. Just, W. Pfleging, and S. Miyazaki, "SMA Microgripper with Integrated Antagonism," *Sensors and Actuators: A*, Vol. 83, 2000, pp. 208-213.

[6] I. Roch, Ph. Bidaud, D. Collard, and L. Buchaillot, "Fabrication and Characterization of an SU-8 Gripper Actuated by Shape Memory Alloy Thin Film," *Journal of Micromechanics and Microengineering*, Vol. 13, No. 2, 2003, pp. 330-336.

[7] E. V. Bordatchev and S.K. Nikumb, "Electro-Thermally Driven Microgrippers for MEMS Applications," *Journal of Microlithography, Microfabrication, and Microsystems*, 4(2), 2005, published on-line May 13, 2005.

[8] C.-P. Hsu, W.-C. Tai, and W. Hsu, "Design and Analysis of an Electro-Thermally Driven Long-Stretch Micro Drive with Cascaded Structure," *Proceedings of the ASME International Mechanical Engineering Congress*, November 17-22, 2002, New Orleans, Louisiana, USA, pp. 235 – 240.

[9] E. V. Bordatchev, S.K. Nikumb, and W. Hsu, Fabrication of Long-Stretch Microdrive for MEMS applications by Ultra Precision Laser Micromachining, *Proceedings of 2002 NRC-NSC Canada-Taiwan Joint Workshop on Advanced Manufacturing Technologies*, Editors: L. Wang, E. Bordatchev, S.-M. Tsay, and S. Lang, 23-24 September 2002, London, Ontario, Canada, pp. 243-252.

[10] Lobontiu, N., *Compliant Mechanisms: Design of Flexural Hinges*, CRC Press, New York, 2003, p.666.

[11] E.V. Bordatchev, S.K. Nikumb, and W. Hsu, "Laser micromachining of the miniature functional mechanisms," *Photonics North 2004: Photonic Applications in Astronomy, Biomedicine, Imaging, Materials Processing, and Education, Proceedings of SPIE*, Vol. 5578 (SPIE, Bellingham, WA, 2004), paper # 5578D-77, pp. 579-588.

[12] M. Zeman, E.V. Bordatchev, and G.K. Knopf, "Electro-Thermo-Dynamic Performance of a Micrograpping System," Proc. IEEE Int. Conf. on Mechatronics and Automation (ICMA '05), 2005, paper MO-A2-04.1.

[13] Y. Lai, E.V. Bordatchev, S.K. Nikumb, and W. Hsu, "Performance Characterization of In-plane Electro-Thermally Driven Linear Microactuators," submitted to *Journal of Intelligent Material Systems and Structures* in June 2005, unpublished.

[14] T A. Faisst, "Determination of the Critical Exponent of the Linear Thermal Expansion Coefficient of Nickel by Neutron Diffraction," *J. Phys.: Condens. Matter*, Vol. 1, 1989, pp. 5805-5810.

[15] T G. Kollie, "Measurement of the thermal-expansion coefficient of nickel from 300 to 1000 K and determination of the power-law constants near the curie temperature," *Physical Review: B*, Vol. 16, No. 11, 1977, pp. 4872-4882.

LIST OF TABLES

Table 1. Comparative analysis of simulated and actual performances.

α_0', β_0' (°, °)	displacements (μm)				transform coefficient (dimensionless)		
	h_{SS}	x_{SS}	$\hat{x}_{SS}$	Δx	$K_{SS} = x_{SS} / h_{SS}$	K	$\Delta K = \lvert K - K_{SS} \rvert$
30, 30	20.0	11.2	11.5	0.3	0.560	0.575	0.015
30, 40	24.1	14.1	14.0	0.1	0.585	0.581	0.004
30, 60	22.3	12.8	13.0	0.2	0.574	0.583	0.009
40, 30	19.0	16.1	15.9	0.2	0.847	0.837	0.010
40, 40	19.2	16.3	16.1	0.2	0.849	0.839	0.010
40, 60	22.4	18.6	18.9	0.3	0.830	0.844	0.014
60, 30	21.2	36.9	36.3	0.6	1.741	1.712	0.029
60, 40	22.4	38.1	38.6	0.5	1.701	1.723	0.022
60, 60	27.8	47.5	48.0	0.5	1.709	1.727	0.018

LIST OF FIGURES

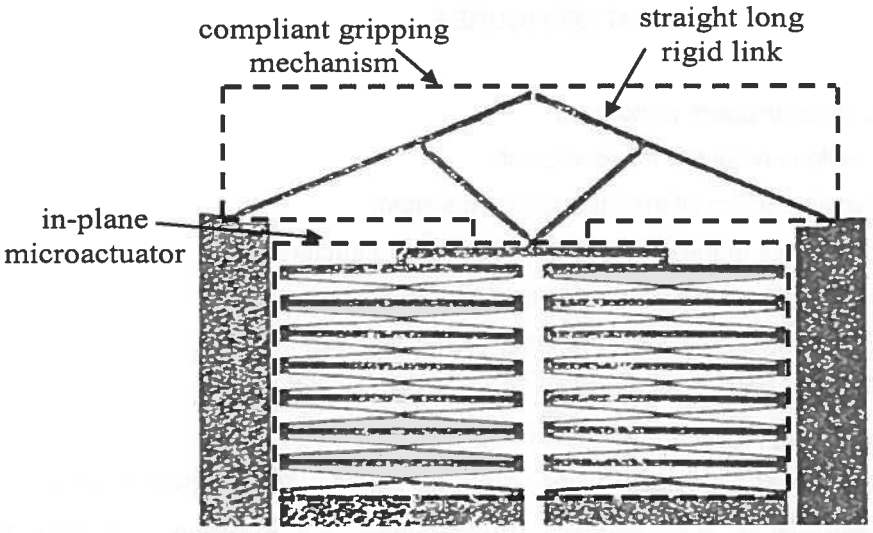

(a) simplified microgripper for comparative kinematic analysis

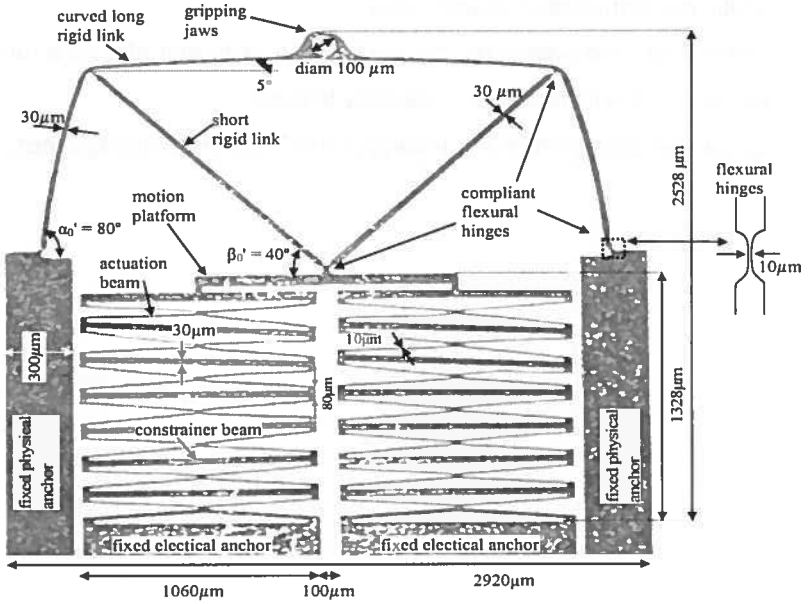

(b) functional microgripper for micromanipulation

Figure 1. Fabricated microgrippers prototypes.

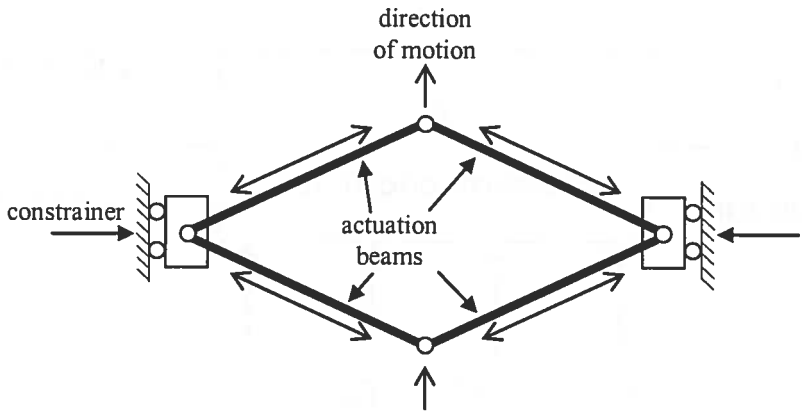

(a) generalized kinematics of the actuation unit

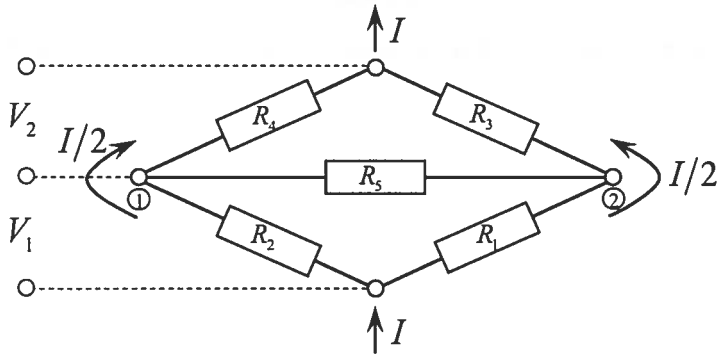

(b) actuation unit mimicking a Wheatstone bridge

Figure 2. Single actuation unit of the microactuator.

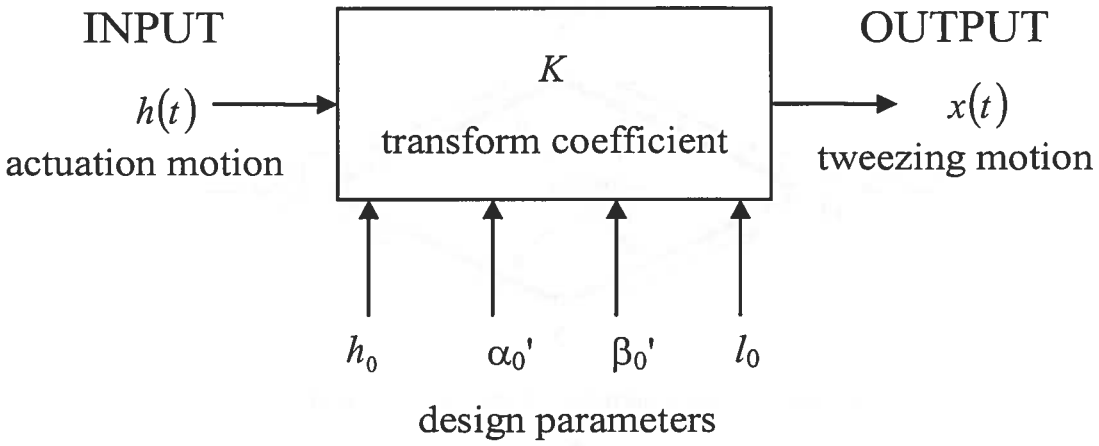

Figure 3. Generalized kinematics of the microgripping system.

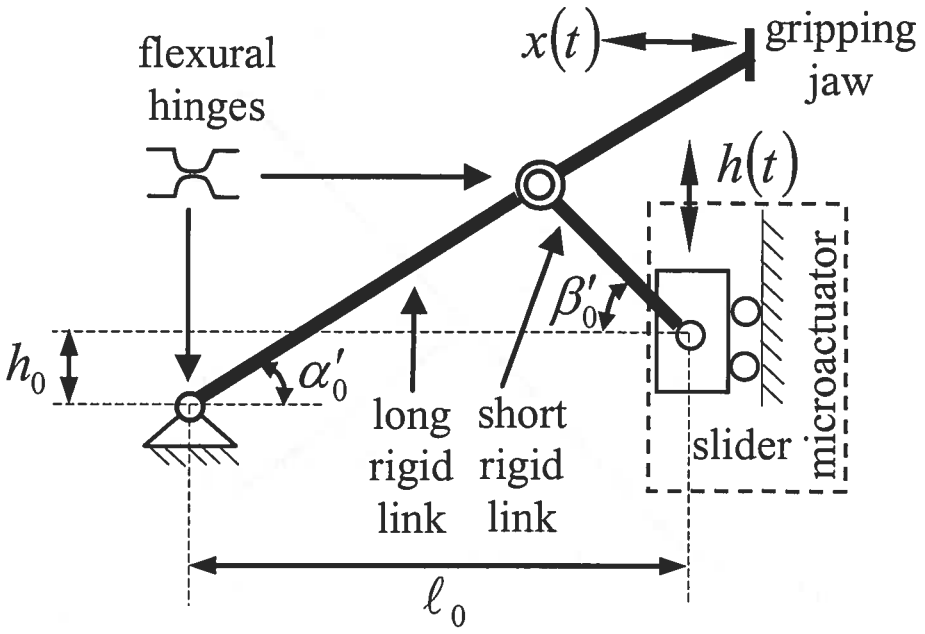

Figure 4. Design parameters of the microgripper's kinematic structure.

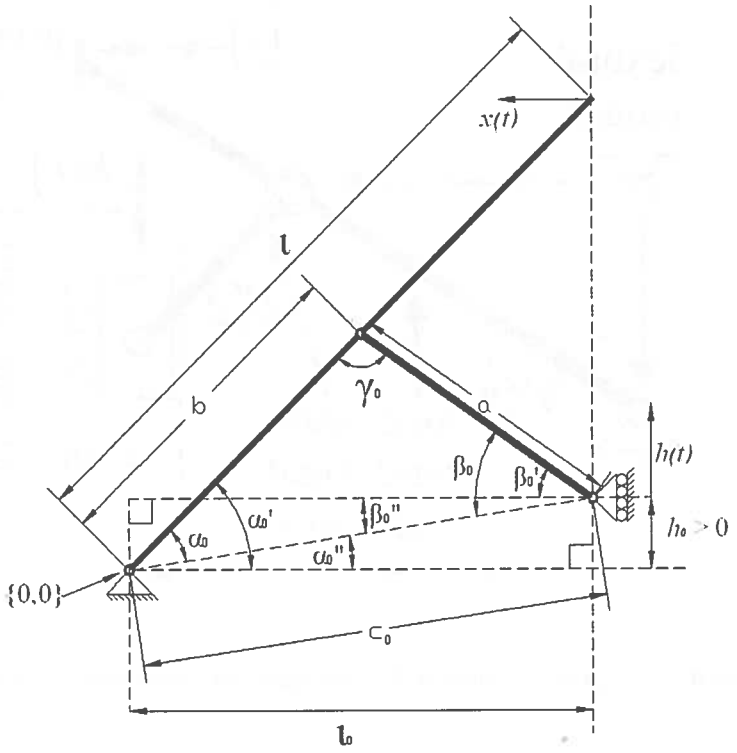

(a) at $t = 0$

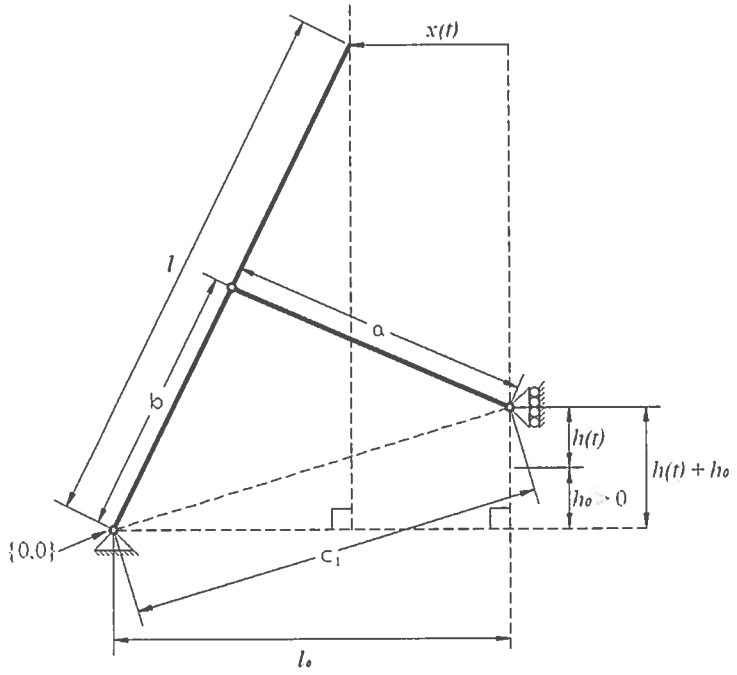

(b) at anytime t after actuation

Figure 5. Detailed kinematics of the microgripping mechanism.

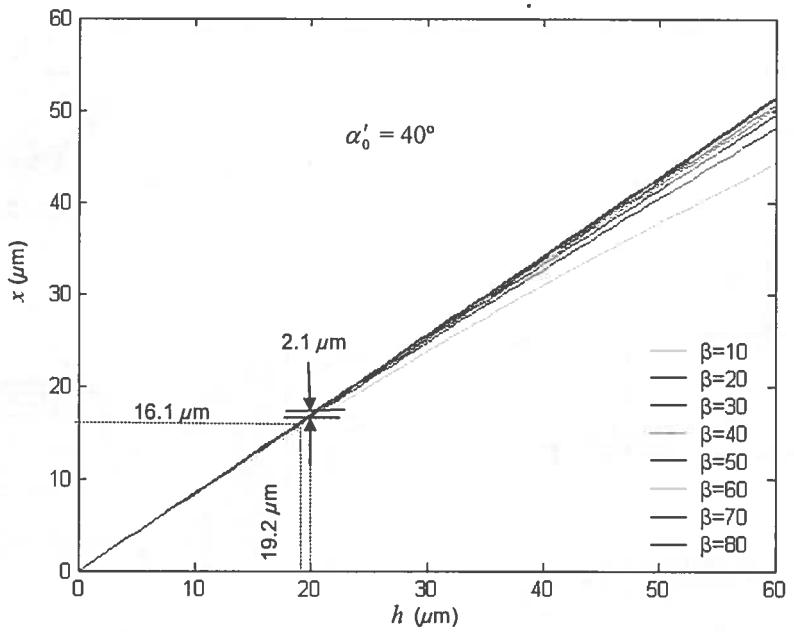

a) performance for h_0 = 0 μm, α_0' = 40°, β_0' = {10°, 20° ... 80°}, and ℓ_0 = 1200 μm

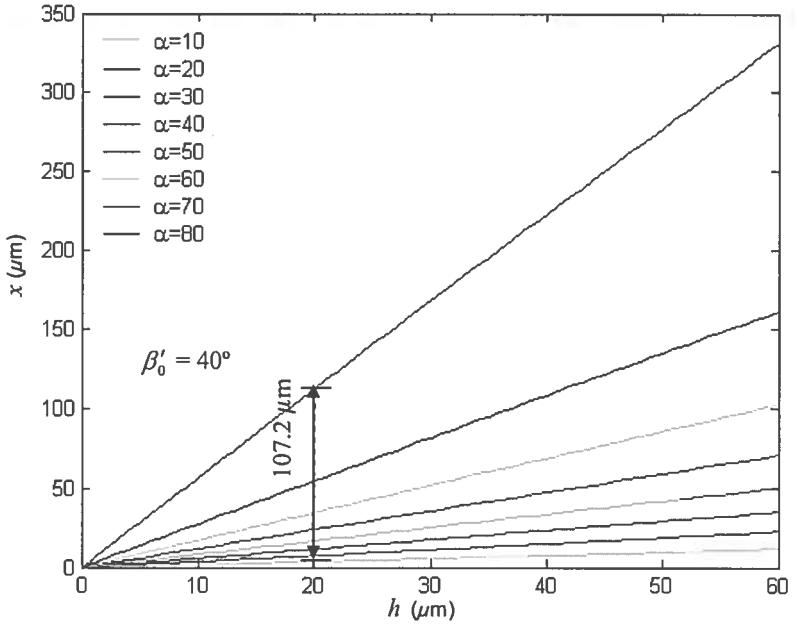

b) performance for h_0 = 0 μm, β_0' = 40°, α_0' = {10°, 20° ... 80°}, and ℓ_0 = 1200 μm

Figure 6. Results on simulation of the microgripper's kinematic performance.

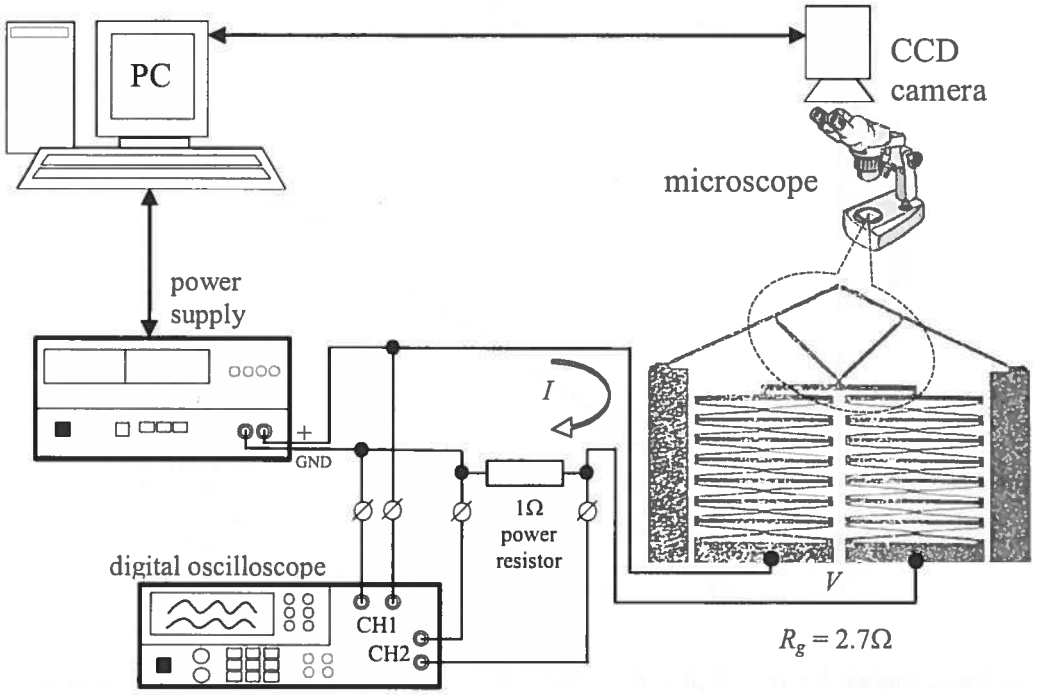

Figure 7. Experimental setup for testing microgripper performance.

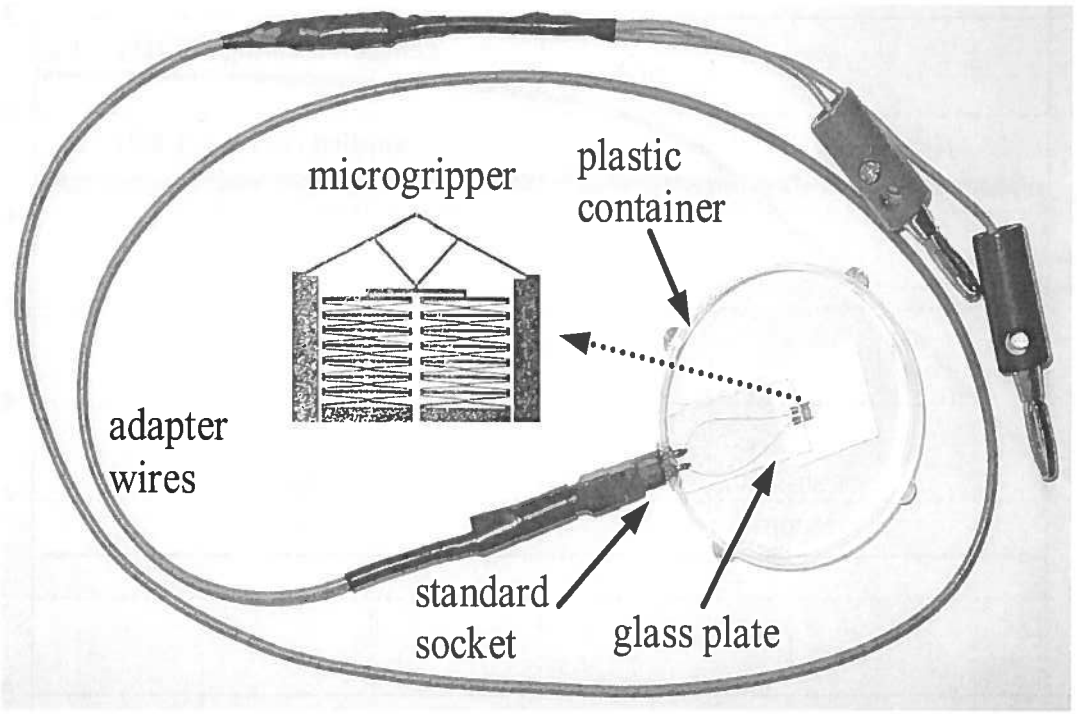

Figure 8. A mounted microgripper with adapter wires.

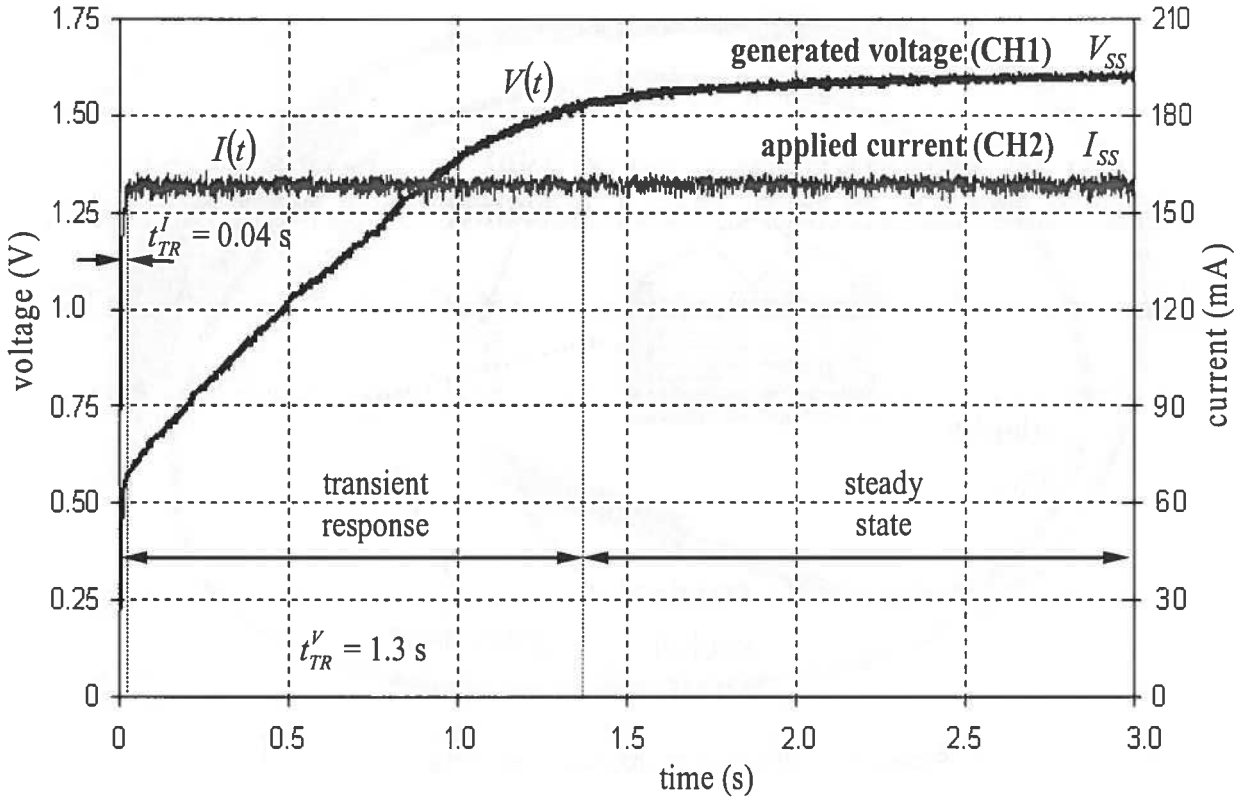

a) electrical step response function

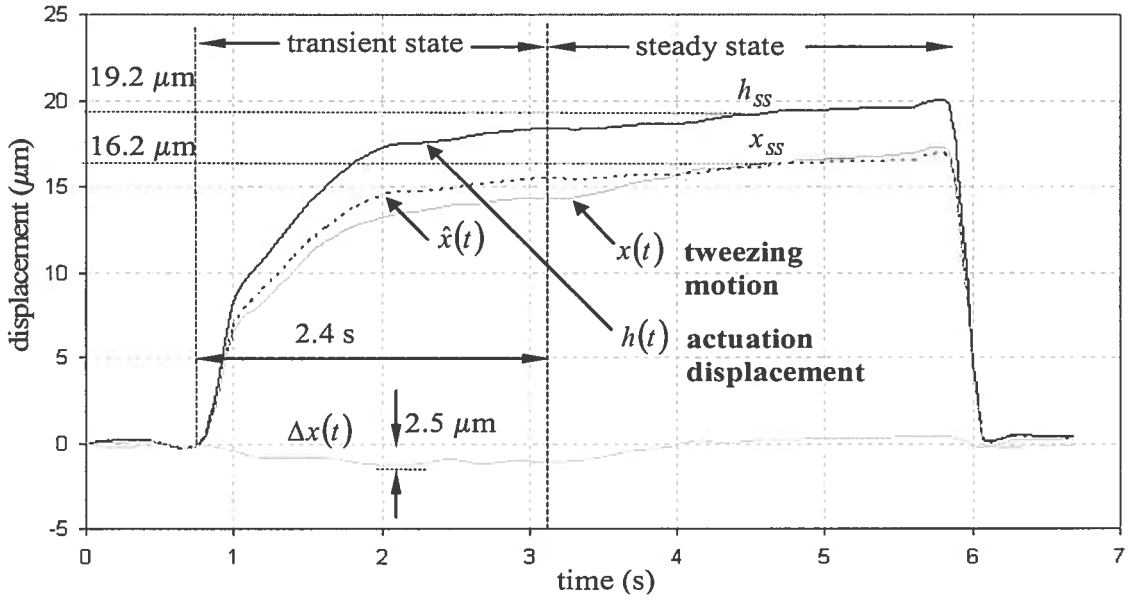

b) mechanical step response function

Figure 9. Typical electrical and mechanical characteristics of microgripper's performance (microgripper with α_0' = 40° and β_0' = 40° and under an applied current of 160 mA).

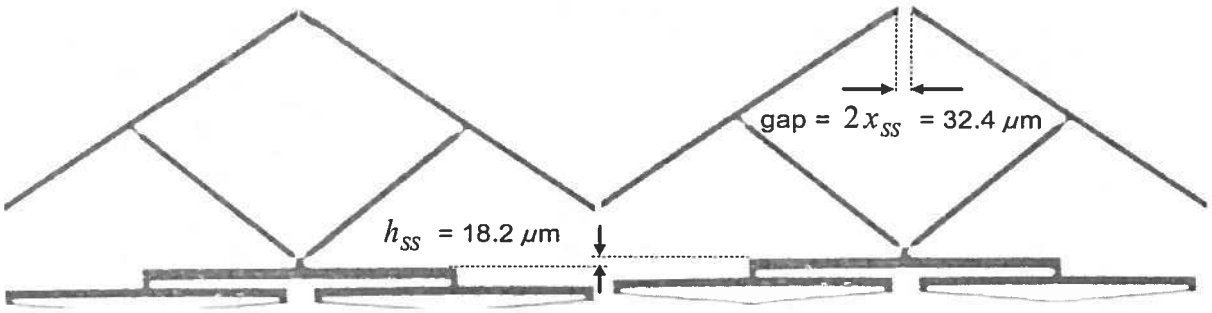

a) closed jaws (initial position) b) opened jaws (steady state position)

Figure 10. Static performance under an applied current of 160 mA.

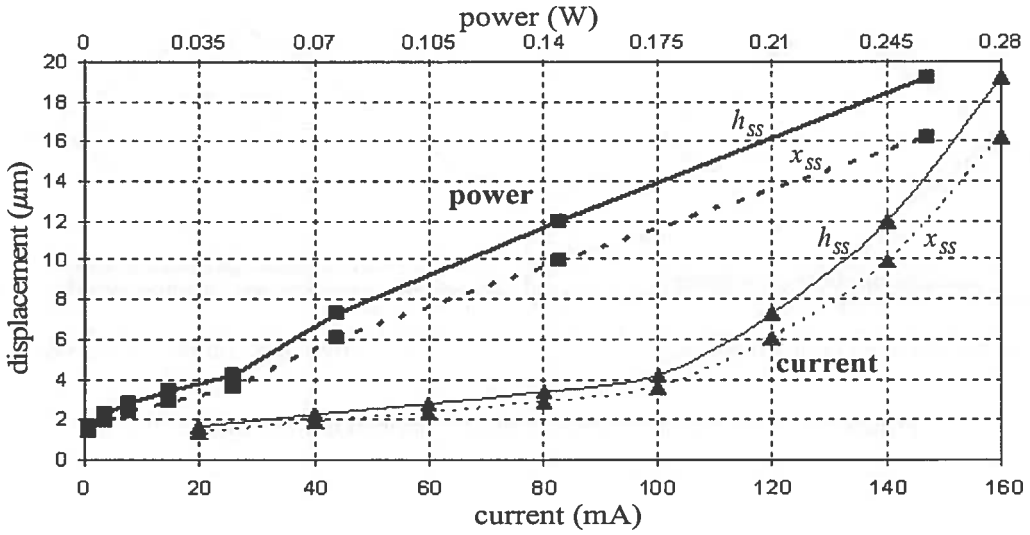

Figure 11. Static performance characteristics.

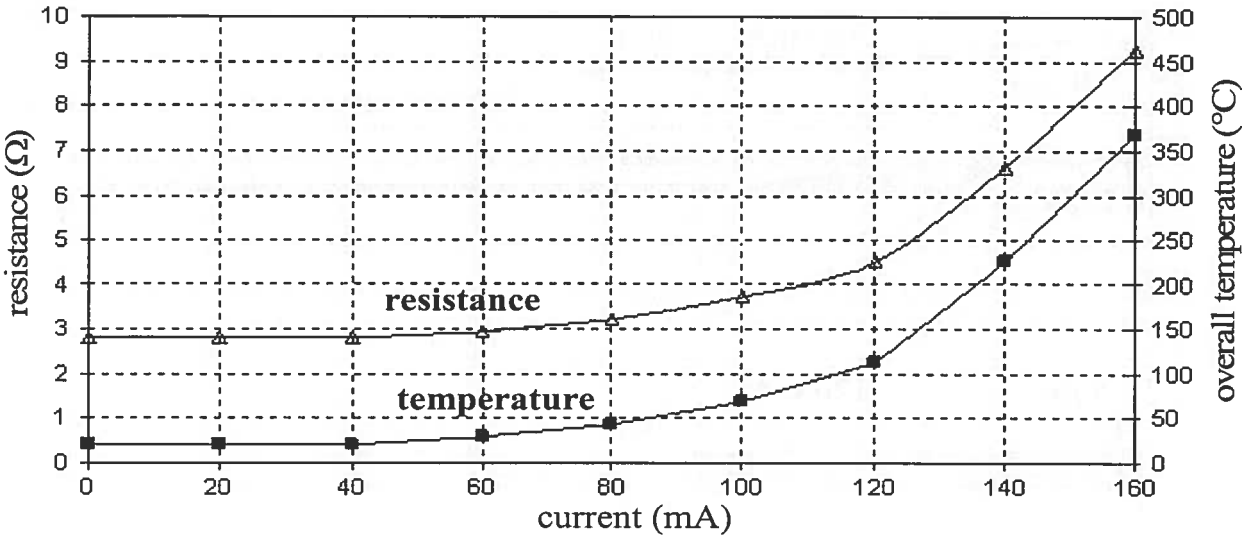

Figure 12. Resistance and overall temperature of the microactuator as a function of current.

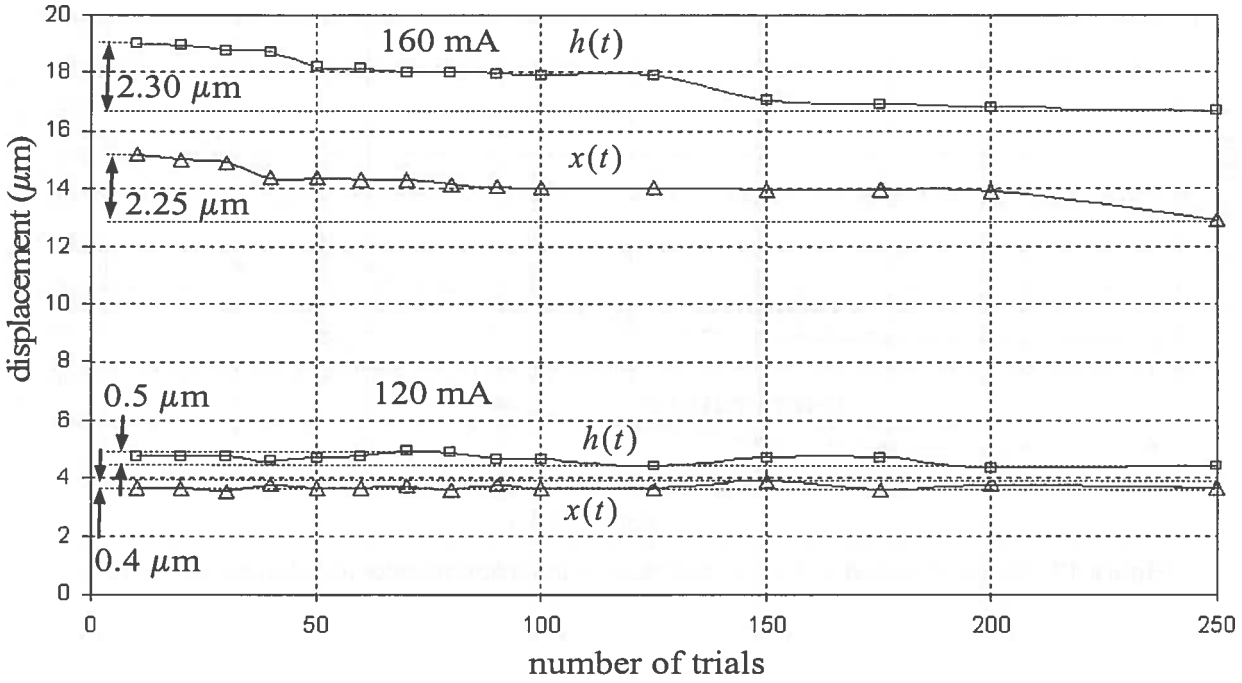

Figure 13. Results of the repeatability/reliability testing.

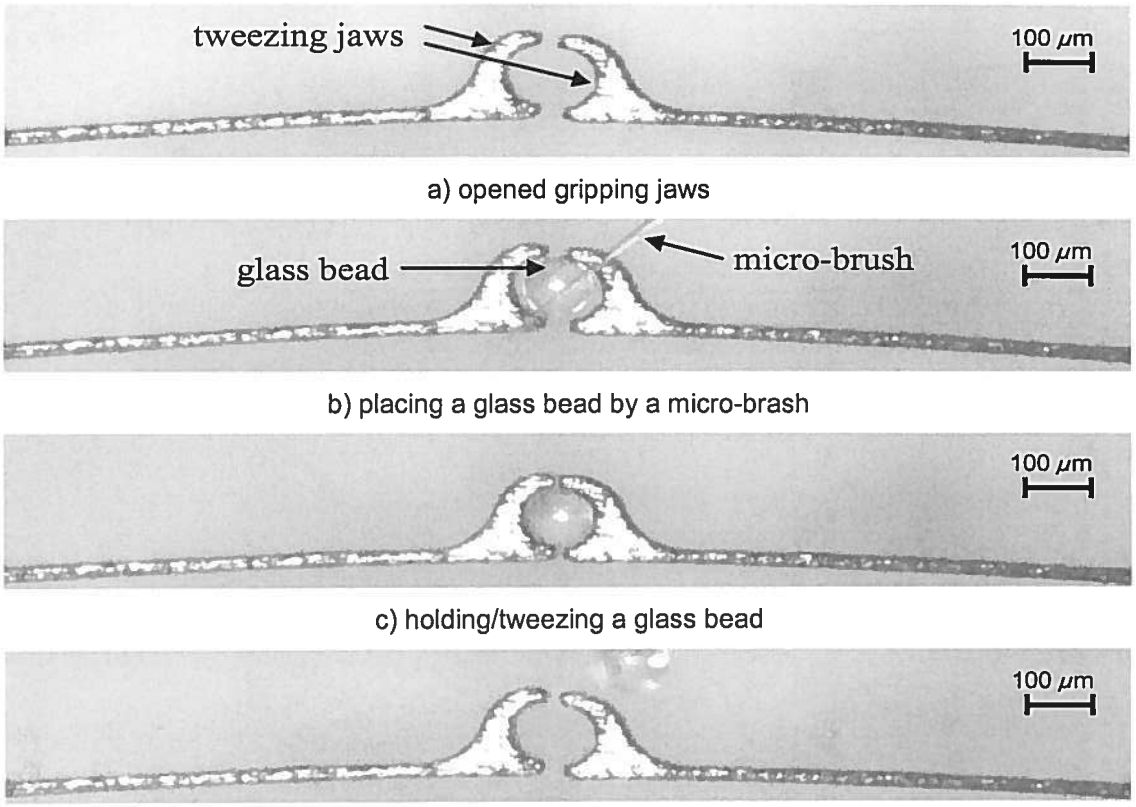

Figure 14. Gripping-holding-releasing testing of the functional microgripper.